A 3D FINITE-ELEMENT MODELLING INVESTIGATION INTO OPTIMAL SURVEY PARAMETERS AND DIRECT IMAGING FOR MARINE CONTROLLED-SOURCE ELECTROMAGNETIC SURVEYS

A Thesis

by

RYAN LAU

Submitted to the Office of Graduate Studies of
Texas A&M University
in partial fulfillment of the requirements for the degree of

MASTER OF SCIENCE

May 2006

Major Subject: Geophysics

A 3D FINITE-ELEMENT MODELLING INVESTIGATION INTO OPTIMAL SURVEY PARAMETERS AND DIRECT IMAGING FOR MARINE CONTROLLED-SOURCE ELECTROMAGNETIC SURVEYS

A Thesis

by

RYAN LAU

Submitted to the Office of Graduate Studies of
Texas A&M University
in partial fulfillment of the requirements for the degree of

MASTER OF SCIENCE

Approved by:

Chair of Committee,	Mark E. Everett
Committee Members,	Thomas A. Blasingame
	Richard Gibson
	David Sparks
Head of Department,	Richard L. Carlson

May 2006

Major Subject: Geophysics

ABSTRACT

A 3D Finite-element Investigation into Optimal Survey Parameters and Direct Imaging for Marine Controlled-Source Electromagnetic Surveys. (May 2006)

Ryan Lau, B.S., University of Waterloo, Canada

Chair of Advisory Committee: Dr. Mark E. Everett

Relatively little is known about marine controlled-source electromagnetic surveys (MCSEM) used to detect hydrocarbon reservoirs. Typical MCSEM require the use of inversion to generate a model of the subsurface. We utilize a 3D finite-element forward model to simulate a MCSEM survey. With the results we were able to determine the strengths and weaknesses of each transmitter and receiver configuration that would best detect a shallow hydrocarbon target. Careful selection of the correct configuration is important as we have found that incorrect transmitter orientation, offset and receiver measurement component can yield misleading results. Using the ideal configuration we were able to directly image the hydrocarbon target without the use of inversion modeling. The direct image is able to show the hydrocarbon target's shape and edges without any ambiguity. The direct image of the target can potentially be used to refine 3D inversion modeling, or be used in conjunction with seismic profiles to refine seismic picks.

ACKNOWLEDGEMENTS

I would like to thank Mark Everett for providing the opportunity to work on such a fascinating topic and also for the continual guidance in the subject matter of marine controlled-source electromagnetics. Also, I would like to thank the various people in the Geology & Geophysics Department with whom I had such insightful discussions with.

TABLE OF CONTENTS

Page

LIST OF FIGURES

INTRODUCTION

Marine controlled-source electromagnetic (MCSEM) surveys have been quickly gaining popularity as a complementary exploration technique to seismic surveys. Its ability to identify whether reservoirs are hydrocarbon bearing or salt saturated is its primary advantage. Up to this point there are relatively few publications on the subject of MCSEM for hydrocarbon exploration (Kong *et al.*, 2002). There is a need for further studies to fill in this gap.

MCSEM had previously been applied only to the study of oceanic lithosphere, active spreading centers, sub-basalt exploration and basin exploration. (Chave and Cox, 1982; Everett and Constable, 1999; MacGregor and Sinha, 2000; MacGregor *et al.*, 2001). These typical MCSEM investigations utilized transmitter and receiver configurations derived primarily from magneto-telluric surveys. As a result, the configurations serve to probe deep crustal targets very well but are less suitable for shallow hydrocarbon targets.

Unlike seismic line profiles where interfaces are visible because of reflections and refractions from a compressional or shear wave, the responses detected by the MCSEM receivers cannot be used for direct interpretation. This has been a big hindrance because MCSEM data requires the use of inversion modeling. Inversion modeling suffers from the problem of taking exhaustive hours along with the inability to determine a unique solution and questionable stabilities of the inversion routine and its results. But, the one main goal of this exhaustive search is to determine a single optimal model which could subsequently be used for interpretation. This shows us that there is a need to determine if direct imaging is possible with MCSEM.

There has been modest success in the development of three-dimensional (3D) controlled-source electromagnetic (CSEM) forward modeling. As a result, very few 3D CSEM forward codes are in existence.

This thesis follows the style of Geophysics.

The majority of the forward modeling codes are 2D or 2.5D. Many of the more advanced 3D codes utilize a finite difference approach that fail to model the seafloor topography because of severe mesh distortions and they are also computationally exhaustive. Everett and Edwards (1993) developed a 2.5D code for time-domain marine CSEM. The other known 2.5D code was developed by Unsworth *et al.* (1993) for 2.5D marine CSEM forward model. His code utilized a 2D conductivity structure that was excited by a 3D horizontal electric dipole source. He contended that many targets may be considered as 2D, (conductivities varying only in 2 directions) greatly reducing the computational costs. Unsworth *et al.* (1993) was able to show the stability of his 2.5D code and the nature of the 3D source interacting with a 2D structure. From what we have discussed here we see all of these forward codes work well only with 2D structures. They lack the ability to model irregular shaped structures.

For this paper we set out to determine if we can directly image a deep water shallow hydrocarbon target. Along the way, we investigate what the best transmitter and receiver configurations are in order to properly probe a hydrocarbon target. This paper utilizes a 3D finite-element forward code developed by Badea *et al*. (2001) to simulate MCSEM surveys. King (2004) had used the code to investigate one component of the electric field. We start off by using the same code that King (2004) had previously used and added two modifications to the code. One was the inclusion of a second measured component of the electric field at the receivers and the other was the ability to alter the orientation of the transmitter. The investigation started off with a study of the individual components of the electric field detected at the receivers. This serves as a starting point to visualize how the responses from each component differ from the others and to see if there were certain components not worth further investigation. After that, we utilize various transmitter configurations and receiver components to investigate the response of a finite disc and a double half-space. Using both responses and along with a simple normalization calculation we are able to generate normalized results to show one edge of a target disc. From these results we are able to identify strengths and weaknesses of each transmitter and receiver configuration. Finally, we used results obtained from the

previous investigation to simulate a MCSEM survey on an incomplete disc target with various survey lines in an attempt to generate a direct image of the subsurface.

METHOD

Marine Controlled-Source Electromagnetics

MCSEM sounding uses a horizontal electric dipole to transmit a discrete frequency electromagnetic signal into the sea and downwards into the seabed. A transmitter is typically towed behind a ship to various offsets at which time an electromagnetic field is emitted from the dipole. The primary electromagnetic (EM) energy is attenuated in the conductive seafloor sediments but once it meets a hydrocarbon reservoir (resistive) the EM energy is weakly attenuated. This allows for propagation within the resistive layer with consistent EM energy leaking back towards the seafloor. An array of seafloor receivers that would have been deployed prior to the start of the survey would then record two orthogonal components of the horizontal electric field (Fig. 1).

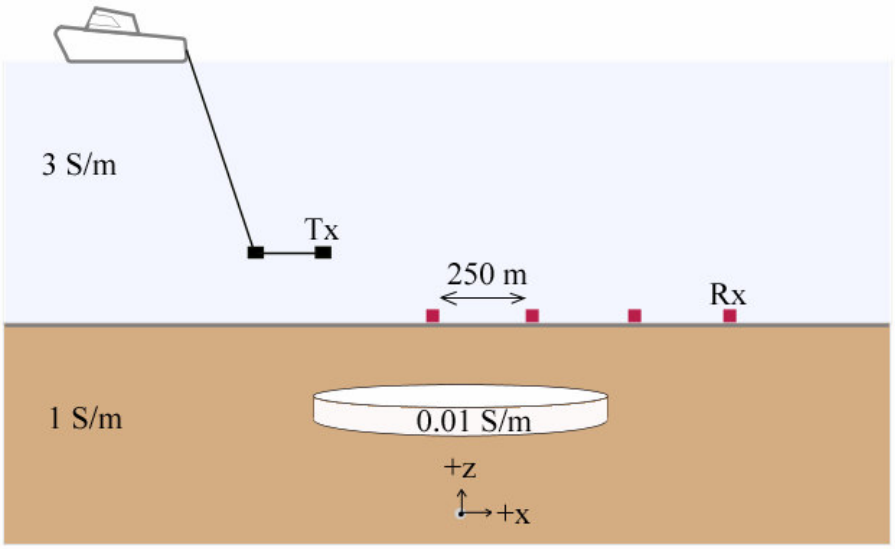

Figure 1. A Typical MCSEM Survey Configuration. Indicated in S/m are the conductivities of the geological medium.

The CSEM method relies heavily on the large resistivity (or conductivity) contrast between the hydrocarbon-saturated reservoirs, and the surrounding saline saturated sedimentary layers. Hydrocarbon reservoirs typically have a resistivity of a few tens of Ωm or higher (conductivity of about hundredths S/m), whereas the surrounding sediments have resistivity of less than a few Ωm (conductivity of about one S/m). This resistivity contrast has a detectable influence on MCSEM data collected by the seafloor receivers even though the hydrocarbon bearing layers are quite thin compared to their depth of burial.

3D Finite-Element Code Background

The 3D finite-element (FE) forward modeling code used for this paper is developed by Mark Everett of Texas A&M university and by Eugene Badea formerly of Haliburton, Inc. The code has been used previously for modeling EM induction well logging in petroleum exploration (Badea *et al*, 2001). The FE method allows for the use of completely unstructured meshes whose edges can be made to conform to irregular geometries that are characteristic of subsurface heterogeneities. We can contrast this to the more popular 3D finite-difference method which requires a structured mesh and do not conform to irregular seafloor topography.

As an alternative to direct electric or magnetic field formulation, Badea *et al.* (2001) formulated the FE EM problem in terms of coupled vector-scalar potentials ($\mathbf{A}$ – magnetic vector potential, ψ - electric scalar potential). The formulation has two conditions which it must satisfy: 1) the tangential component of the electric field is the only component that can cross continuously though the interface of any two media, while the normal component is discontinuous and 2) the calculated EM fields contain no divergent spurious modes. The Coulomb-gauge potential was first developed by Biro and Preis (1989). The first condition is met using gauge potentials since the magnetic vector potential $\mathbf{A}$ and electric scalar potential ψ are both continuous across interfaces. Furthermore, when the Coulomb gauge condition is enforced via the equation $\nabla \cdot \mathbf{A} = 0$ it ensures that there are no divergent spurious modes.

We will show a simplified version of the derivation of found in Badea *et al*. (2001). Maxwell's diffusion equation shown in equations 1 and 2 which the Gauge EM potentials are developed from, are valid only for low frequencies. The low frequency requirement is governed by $\sigma << \varepsilon\omega$ (σ - electrical conductivity, ε - electric permittivity, and ω - angular frequency). In addition, for equations 1 and 2, μ_0 is the permeability of free space, and $\mathbf{J}_s$ is the electric current density of the source.

$$\nabla \times \mathbf{E} = i\omega\mu_0\mathbf{H}, \tag{1}$$

$$\nabla \times \mathbf{H} = \mathbf{J} = \mathbf{J}_s + \sigma\mathbf{E}. \tag{2}$$

Badea *et al*. (2001) first applied $\mathbf{B} = \mu_0\mathbf{H}$ to relate the magnetic induction and magnetic field vectors, then imposed both $\nabla \cdot \mathbf{J} = 0$ and $\nabla \cdot \mathbf{B} = 0$ to ensure the solution was source and sink free.

Equations 1 and 2 can be solved more readily if **E** and **H** is expressed in terms of a magnetic vector potential **A** and an electric scalar potential Φ defined from the following pair of equations:

$$\mathbf{B} \equiv \nabla \times \mathbf{A}, \tag{3}$$

$$\mathbf{E} \equiv i\omega\mathbf{A} - \nabla\Phi. \tag{4}$$

Applying the two EM potential equations from (3) and (4) into (2) produces:

$$\nabla \times \nabla \times \mathbf{A} = \mu_0\mathbf{J}_s + \mu_0\sigma(i\omega\mathbf{A} - \nabla\Phi). \tag{5}$$

Badea *et al*. (2001) then proposed we follow an approach proposed by Biro and Preis (1989) and incorporate the term $-\nabla(\nabla\cdot\mathbf{A})$ to the left side of equation 5 to avoid asymmetric FE matrices. The asymmetric matrices could cause numerically unstable modes. The result of this is:

$$\nabla \times \nabla \times \mathbf{A} - \nabla(\nabla\cdot\mathbf{A}) - i\omega\mu_0\sigma(\mathbf{A} + \nabla\Psi) = \mu_0\mathbf{J}_s \tag{6}$$

The added term vanishes leaving equation 5 unchanged as long as the condition $\nabla \cdot \mathbf{A} = 0$ is satisfied. A vector identity $\nabla \times \nabla \times \mathbf{A} - \nabla(\nabla \cdot \mathbf{A}) = -\nabla^2\mathbf{A}$ is applied by Badea *et al*. (2001) showing that equation 6 is equivalent to a vector Helmholtz equation

$$\nabla^2 A + i\omega\mu_0\sigma(\mathbf{A}+\nabla\Psi) = -\mu_0\mathbf{J}_s \tag{7}$$

The divergence of equation 5 was done to show that the divergence-free condition $\nabla \cdot J = 0$ is automatically enforced. Problems arise with the solution not being source free if the augmented equation 6 is used. Badea *et al*. (2001) found that in order to maintain a divergence-free current density, the auxiliary equation 8 must be solved simultaneously in conjunction with the Helmholtz equation.

$$\nabla \cdot [i\omega\mu_0\sigma(\mathbf{A}+\nabla\Psi)] = 0 \tag{8}$$

Previous Studies

King (2004) was the first to utilize the code developed by Badea *et al*. (2001) as a MCSEM FE model. He first validated the code by comparing double half-space responses between the 3D code and an analytically solved 1D code. Results between the two codes match fairly well once the mesh sizes of the FE code were altered slightly. The remainder of King's (2004) experiments was focused on a parametric study of the 3D FE code. For the simple parametric studies, a model of a double half-space consisting of the sea for the top half and seafloor sediments for the bottom half was the starting point. A conductive disc was also embedded within the seafloor sediments. King's study utilized only the x-component of the electric field detected by the receivers along the x-axis of the FE mesh with a transmitter oriented in an inline configuration which was collinear with the receiver array. With the transmitter fixed in place, frequencies were varied from 0.005 to 1.0 Hz. At each frequency multiple simulated surveys would be conducted with no disc, and later with an inserted disc of various radii up to an infinite disc size. It was found that at one fixed frequency, as the disc size increased it behaved like an infinite disc at close receiver positions, while at far receiver positions the disc response behaved as if it was a double half-space. As the frequencies were altered several additional conclusions could be made based on frequency selection. The selection of frequency should depend strongly on the depth of the target. High frequencies are subjected to excessive attenuation and thus can only probe fairly shallow depths. In the other end of the spectrum, low frequencies are more suitable for deep targets. Incorrect selection of the frequency can lead to either probing above or below the target. Investigations into the placement of the transmitter proved to be also

insightful. When the transmitter was located near or directly over the target, the near receivers could not provide a distinction between an infinite disc and a double half-space. However as we move to further along to different receivers a clearer separation between the infinite disc and the double half-space could be seen before the infinite disc grades into the double half-space response at far receivers. Subsequent placement of the transmitter at further and further locations showed that its position controlled the location where there would be a clear separation between the infinite disc and double half-space.

The final part of King's (2004) investigation utilized a complex hydrocarbon structure shape roughly similar to that of an anticline. It was constructed with three different discs of varying radii and shape. King (2004) was able to determine that the ideal frequency was 0.1 Hz because it exhibited the most consistent and greatest separation between the structure's response and a double half-space response. The last part of this investigation was an attempt to locate the shallowest part of the reservoir where ideally most of the hydrocarbon would accumulate. In King's (2004) studies he was not able to locate the shallowest part of the reservoir but he was able to find that the 3D nature of the structure can be observed with the detected responses.

Transmitter-Receiver Nomenclature

A brief discussion on the nomenclature of the transmitter and receiver configurations is needed due to the number of different possible scenarios. As illustrated in figure 2, the transmitter is a horizontal electric dipole (HED). It is moved along the x-axis to various locations and positioned 100 m above the seabed. There are two orientation modes for the transmitter: inline and broadside. The inline orientation (Fig. 2a) is when the transmitter dipole is collinear to the x-axis (X-HED) while the broadside orientation (Fig. 2b) is when the dipole is parallel to the y-axis (Y-HED). Since an HED was utilized for the transmitter, the receivers are measuring the horizontal components of the electric field. On the x-axis, two orthogonal components of the horizontal electric field are measured. The E_x component on the x-axis is called the EXEX and E_y

component of the electric field on the x-axis is called EXEY. On the y-axis, the only measured component is the E_y which we name EYEY.

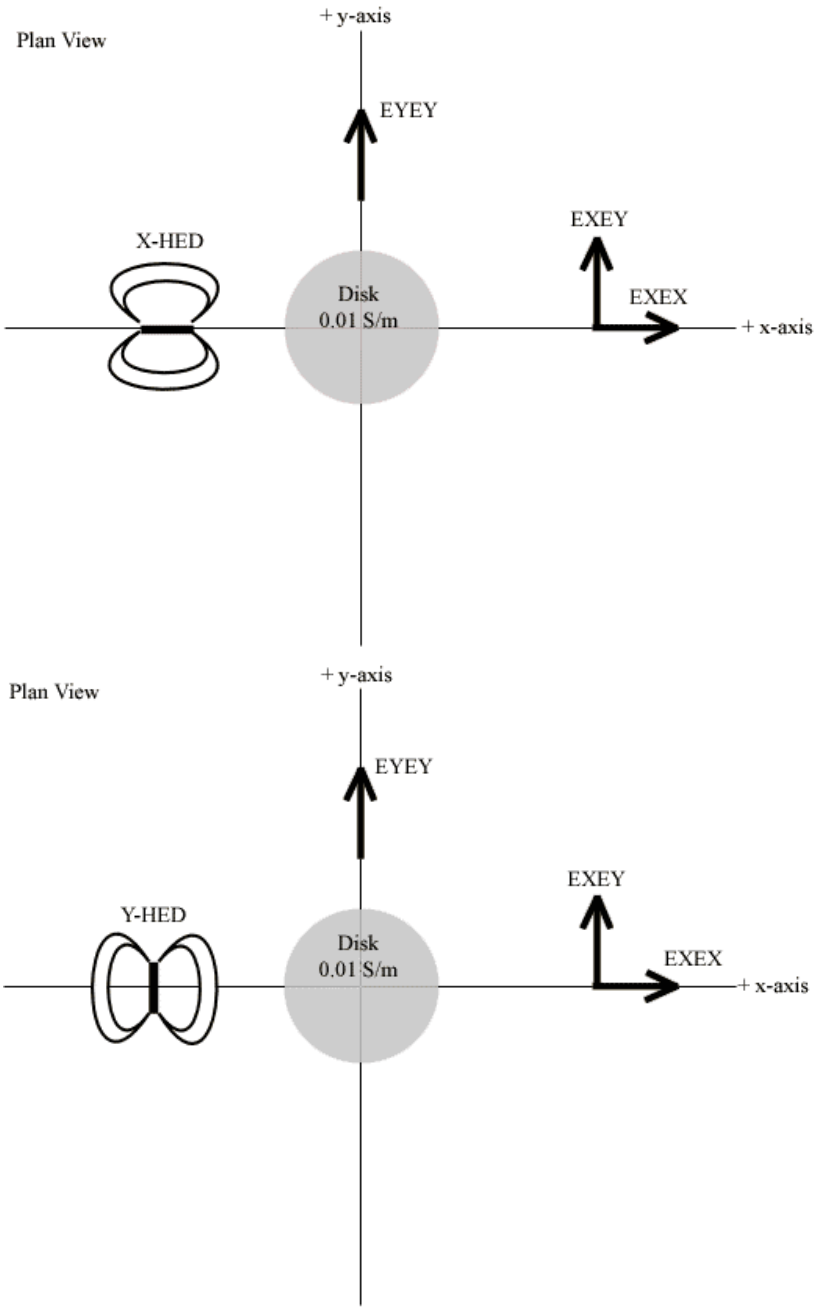

Figure 2. Transmitter and Receiver Configuration. (a) X-HED transmitter configuration (b) Y-HED transmitter configuration.

RESULTS

EXEY and EYEY Investigation

In our first experiment we investigated the EXEY and EYEY components with an X-HED transmitter orientation. The goal was to establish if the other electric field components could detect a hydrocarbon disc target and if so, are there any differences that can be identified when compared to the EXEX case. The X-HED EXEX transmitter-receiver scenario had been previously investigated by King (2004) and it served as a starting point.

A geological model was constructed for this investigation (Fig. 1). The starting model is a double half-space consisting of an overlying seawater layer of 1 km depth with a conductivity of 3 S/m and an underlying infinite half-space consisting of seawater saturated sediments with conductivity of 1 S/m. The study required the use of various hydrocarbon discs centered in the middle of FE mesh with electrical conductivity of 0.01 S/m and embedded at 525 m depth within the seawater saturated sediments. The disc had a thickness of 32 m and the radius ranged from: no disc present, 1250 m, 2500 m, 5000 m and an infinite disc. Two arrays of thirty-two receivers with a separation of 250 m are placed on the positive x-axis and y-axis beginning from 0 m and extending to +7500 m. The array on the y-axis measures only the E_y component of the electric field while the array on the x-axis measures both E_x and E_y components. The transmitter was placed with an X-HED orientation at a fixed position of -1000 m on the x-axis, at a height of 100 m above the seafloor and with an operating frequency of 0.1 Hz.

The results for the EXEY and EYEY is plotted in Fig. 3. The response of the EXEY in Fig. 3a has amplitudes between $10^{-13.5}$ and 10^{-18} V/m. A typical estimate of background seafloor EM noise levels encountered in practice is less than $10^{-14.5}$ V/m. It is clear that given the EXEY response is well into the accepted noise level; it would not be suitable for MCSEM investigations. The EYEY response in Fig. 3b shows a strong response similar to that of EXEX. From the separation of responses of the double half-space and disc curves, the EYEY shows a clearer distinction of when a disc is present for short range receivers up to 2 km before disc response grades into a double half-space

response. In contrast the EXEX is only able to show a separation at distances under 1km along with a short separation visible beyond 1 km. The responses of both EXEY and EYEY have been shown here, it is clear that the EXEY need not be investigated further. The EYEY response demonstrated that it can clearly detect the disc, providing responses well above the background EM noise level and could potentially be a better indicator for disc imaging.

Normalization Investigation

Our investigations expanded as a result of the previous experiments which indicated that the EYEY components should be investigated further. Up to this stage no publications for MCSEM had been completed on the EXEX and EYEY response when the transmitter was rotated ninety degrees into the Y-HED orientation. From various transmitter and receiver configurations, we set out to determine the most favorable configuration that would allow for direct imaging of the subsurface.

A similar geological model to the EXEY and EYEY investigation was used for the normalization investigation. The same double half-space parameters such as thickness, and conductivity were used. The only difference in this investigation was that we used only a 2500 m radius disc centered in the middle of the FE mesh with a thickness of 32 m and depth of 525 m. No other different radii discs were used in this investigation. The two receiver arrays are still in the same position as described in the previous investigation; along the positive x-axis and y-axis. The transmitter configuration is the main parameter which varied in this experiment. At each discrete frequency between 0.005 to 1.0 Hz, the transmitter position was kept at 100 m above the seafloor and moved along the x-axis to -1000 m, -1500 m, -2000 m, -2500 m and -3000 m. Two simulated responses were taken at each position with the 2500 m disc present and with a double half-space. This simulation was done for both the X-HED and Y-HED.

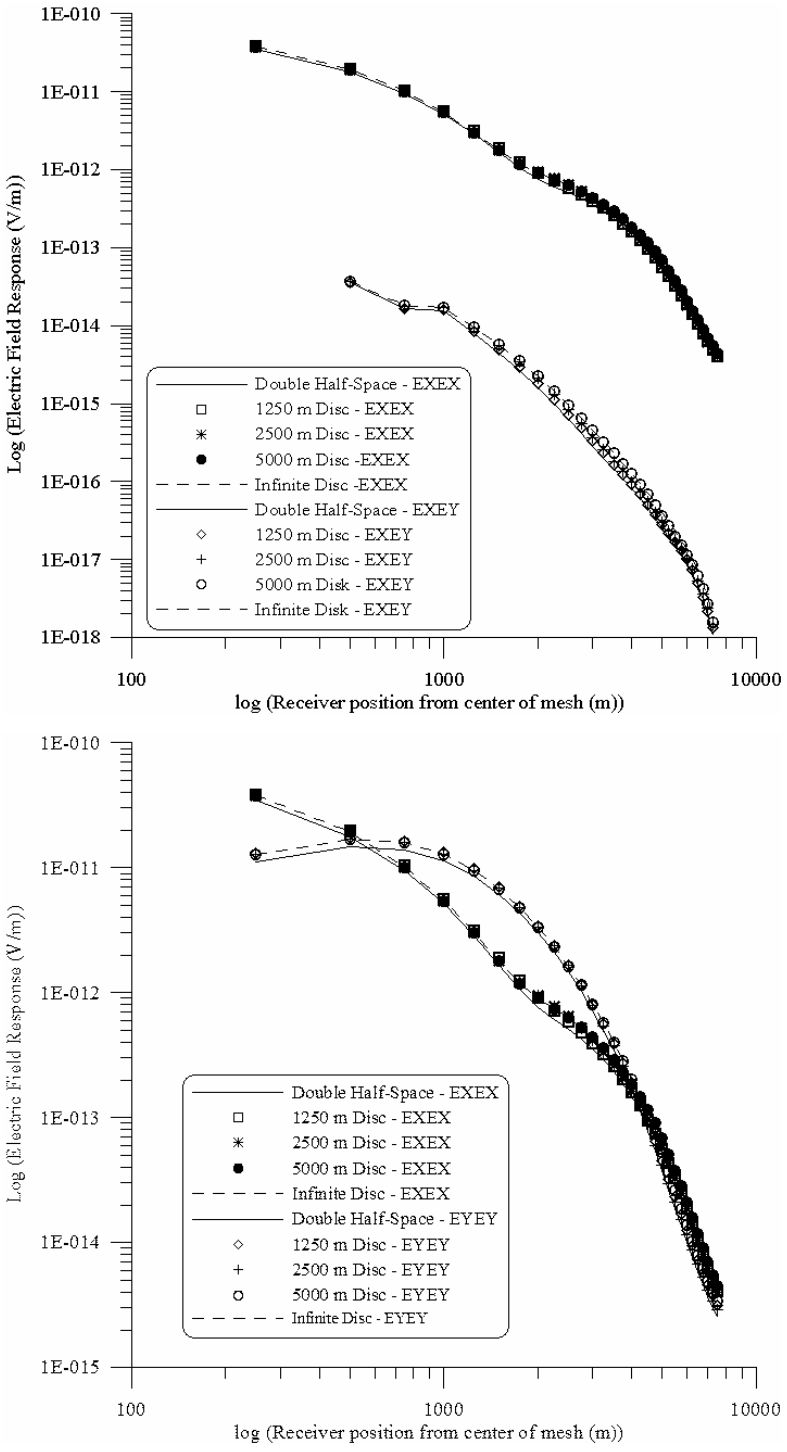

Figure 3. Synthetic X-HED EXEY and EYEY Results. (a) X-HED EXEY and (b) X-HED EYEY compared to X-HED EXEX both with transmitter located at -1000 m and with a frequency of 0.1 Hz.

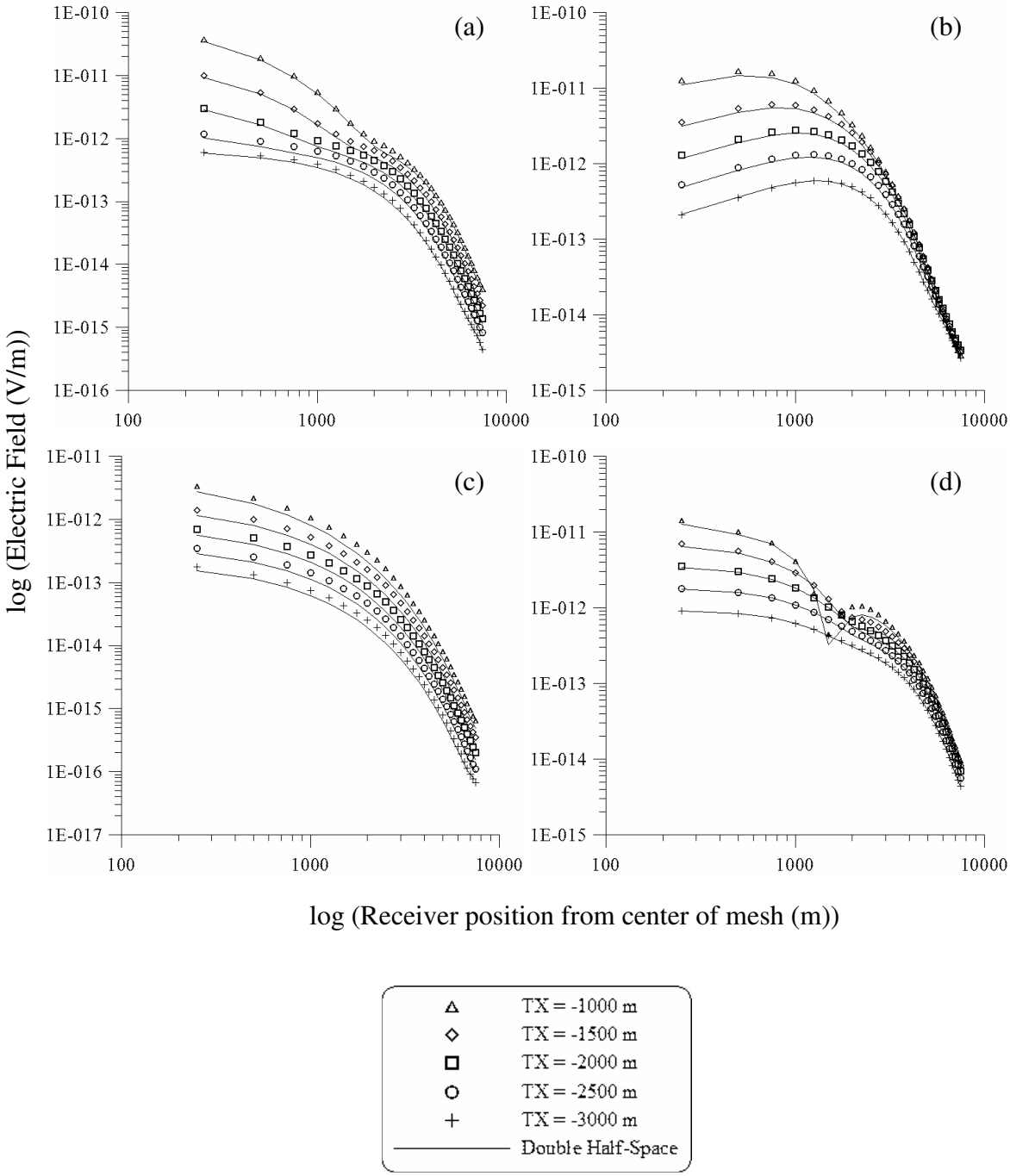

Figure 4. Synthetic Results of Normalization Investigation. (a) X-HED EXEX; (b) X-HED EYEY; (c) Y-HED EXEX; and (d) Y-HED EYEY. Symbols represent the disc response for five sequentially further transmitter positions away from the center of the disc on the negative end of the x-axis. While the overlapping lines represents the corresponding double half-space response at the same transmitter positions.

The raw synthetic data presented in Fig. 4 are plotted based on different transmitter positions. We have presented only the 0.1 Hz transmitter frequency in this paper. All four plots show a clear indication that the signal grades into weak double half-space responses at far receiver positions. One key point that will never change regardless of configuration is that as the transmitter is towed further away from the receiver array, the response strength declines sequentially.

As found by King (2004) the X-HED EXEX suffers from the problem of close transmitter positions not being able distinguish between the disc and double half-space at near receivers. While at farer transmitter positions the receivers is able to distinguish between the double half-space and finite disc. The X-HED EYEY does not suffer from such limitations as what we had just described. With the exception of the furthest transmitter position, receivers up to 3 km away from the center of the mesh show a clear separation between the finite disc and the double half-space. Beyond the 3 km mark all the responses from all transmitter positions converge together, indicating a similar double half-space response shared by all transmitter positions.

Once the transmitter orientation has been rotated into the Y-HED configuration there are significant changes in the results. The Y-HED EXEX configuration clearly demonstrates it not subjected to same constraints as what we have seen in the X-HED. There is a clear separation between when the finite disc and the double half-space at each different transmitter position for near and far receiver positions. It is noticeable that disc response does not grade into a double half-space response until 6 km from the center of the mesh in this configuration. The synthetic curves from 0.005 to 1.0 Hz all look exactly the same as to what was is shown in Fig. 4c, with disc and double half-space separation consistently visible. In Fig. 4d which shows the Y-HED EYEY it can be seen that at the transmitter position of -1000 m a small minimum occurs at receiver position of 1500 m. With the exception of 0.1 Hz, this anomaly is visible at all transmitter positions at frequencies ranging from 0.005 Hz up to 0.05 Hz. The minimum occurs as a result of a null coupled configuration between the transmitter and receiver. The null coupled position arises at the cusp of the field lines. In this zone it is a

quiescent area where any receivers located in this area would not detect the primary electric field from the source. Receivers in the null position would therefore only detect the secondary field generated by the conductive target. Under normal circumstances this null coupled position can be used to our advantage because outside of this position, receivers detect a superimposed response of the primary and secondary fields. Our investigation was not interested in utilizing the null coupled configuration, meaning that it cuts out a large range of frequencies which cannot be used due to the null coupled problem. For this transmitter and receiver configuration we are able to separate the response of the finite disc and the double half-space at all receiver positions with the exception of the far locations where the disc response grades to a double half-space response. However, it is noticeable that the separation between the two responses is greatest at moderate positions.

The problem with the synthetic data is that it cannot be used as a visual map for direct interpretation of boundaries as compared to seismic lines where reflectors typically indicate some type of interface. This problem is inherently due to the nature of EM fields which unlike primary waves (P-waves) that bounce off interfaces, EM fields flow though interfaces as though sharp boundaries are not present. To overcome this problem, the synthetic data was normalized in an attempt to isolate the response of the disc and to image one edge of the target disc. The normalization of the data required two responses to be known. One is obviously the response with the disc in the double half-space and the other is just the double half-space. To correctly normalize the data, both responses must have the same transmitter parameters: its frequency, orientation, and transmitter-receiver offset must all be the same. The normalization uses the following equation:

$$\text{Normalized Response} = \frac{[\text{Disc Response} - \text{Double Half-space Response}]}{\text{Double Half-space}} \qquad (9)$$

From equation 9, it should be expected that when a disc is present a positive non-zero normalized response should be yielded, while in the absence of any disc we should get a value of zero.

As seen from the synthetic results shown in Fig. 4, selected normalized plots are presented in Fig. 5. The normalized results show the frequent occurrence of an isolated peak in the vicinity of the edge of the disc for selected transmitter-receiver configurations.

King (2004) described the importance of correct selection of transmitter position. From Fig. 5a, the X-HED EXEX can be seen to have normalized response strength dependant strongly on the location of the transmitter. Transmitter positions on the edge or within the disc provide stronger normalized responses than compared to when it is located outside the disc. Frequencies from 0.005 Hz – 0.05 Hz either did not have a strong isolated peak, or the peak was incorrectly aligned. For cases where a peak was visible, the necessity of selecting the correct transmitter position is needed to be known. We suspected that by moving the transmitter further away it offset the problem of the low frequencies having deep skin depths which were well beyond the 525 m depth of the disc. One issue that plagues this configuration is that at far receiver positions the normalized response is non-zero. For these far receiver positions, the response of the secondary field generated by the disc is still weakly visible but not as prominent as the peak indicating the edge of the disc.

The X-HED EYEY had similar characteristics to the EXEX case. Peaks are visible; however in the cases where the source frequency was less than 0.5 Hz, it was overshadowed by strong surrounding normalized responses from the far receivers. The transmitter position in this configuration as what was described in the synthetic results did not control the position of the edge peak of the disc. Where the peak was visible, it consistently had correct alignment. But, the transmitter position similarly as in the EXEX controls the strength of the normalized peak. Transmitter positions on or within the disc closest to the edge yielded the best results, followed by a decline in strength with further transmitter positions outside the disc.

The Y-HED EXEX where in the synthetic results showed the same features at all frequencies, the normalized response produced similar results as expected. Clear and isolated peaks all correctly aligned at the position over the edge of the disc regardless of what frequencies were chosen. The strength of the normalized responses in this configuration scenario favored transmitter positions which were inside the disc and near the edge, while at the position directly over the edge and further outside the disc declined sequentially.

The Y-HED EYEY in Fig. 5d-f we showed frequencies from 0.1 to 0.5 Hz. As discussed previously, this configuration is subjected to the presence of null coupled positions. At frequencies below 0.1 Hz, the null coupled problem dominates the normalized responses and create peaks where there should be no peaks. At the transmitter position of -1000 m in the 0.1 Hz plot; note that we did see a null coupled response in the synthetic data in Fig. 4d. The null coupled position has caused the peak in Fig. 5d to be incorrectly aligned, whereas the other transmitter positions had correctly aligned peaks. Unlike from what was described in the previous configurations the strength of the normalized response peaks for the Y-HED EYEY correspond only to the transmitter-receiver array offset. The smaller the offset between the two yields the strongest response, with a sequential decline in strength at larger offsets. This potentially means that unlike the previous three configurations, the presence of the disc does not control the strength of the response rather that only the offset between the two is the main contributing factor.

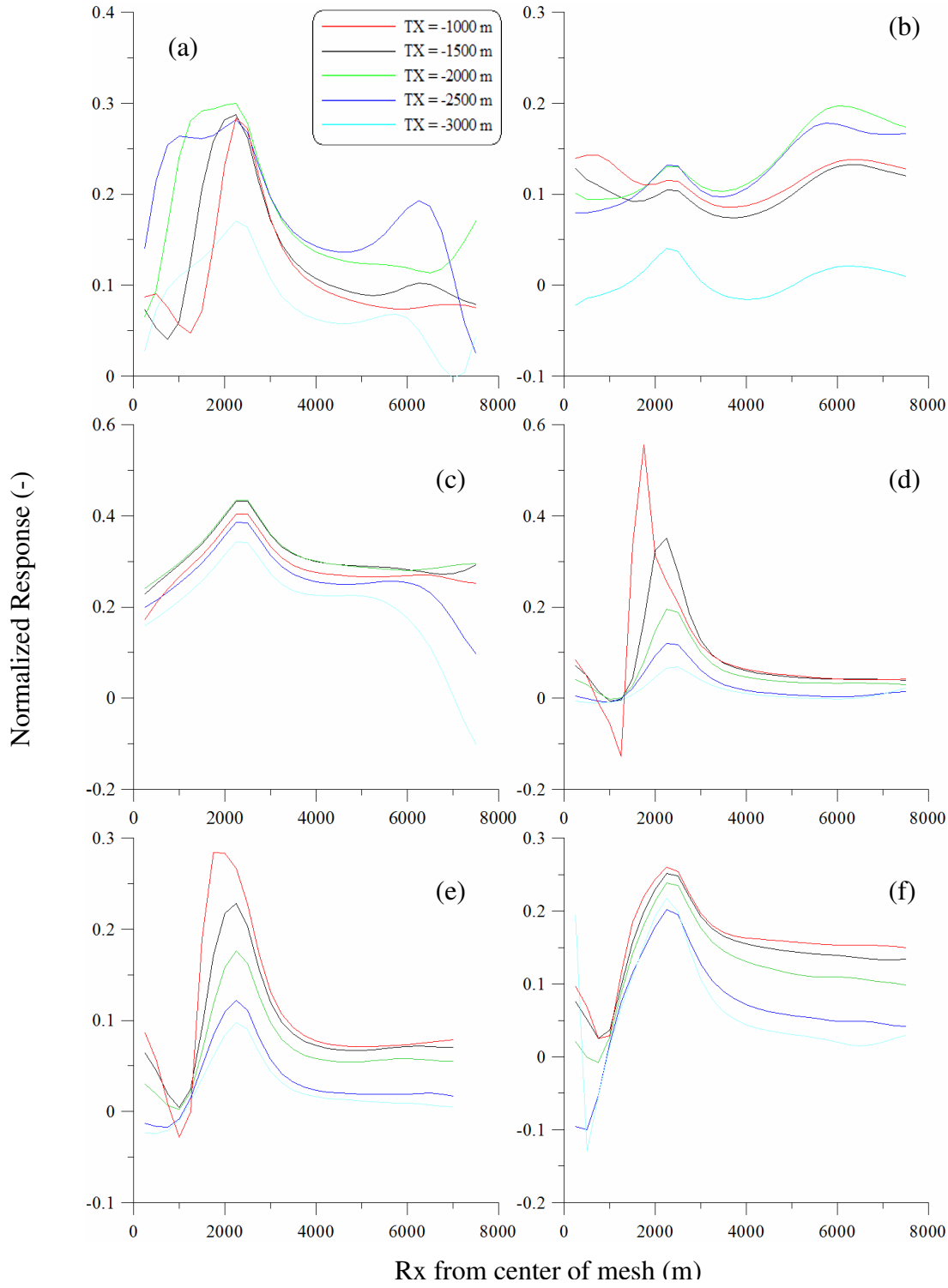

Figure 5. Normalized Synthetic Results. (a) X-HED EXEX f = 0.1 Hz; (b) X-HED EYEY f = 0.1 Hz; (c) Y-HED EXEX f = 0.1 Hz; (d) Y-HED EYEY f = 0.1 Hz, (e) Y-HED EYEY f = 0.2 Hz, (f) Y-HED EYEY f = 0.5 Hz.

The results of what has been discussed in the normalized investigation have been recorded in Table 1. For each transmitter orientation and receiver component, an ideal transmitter operating frequency and position has been tabulated. These configurations will work well for identifying one edge of shallow hydrocarbons targets buried within a 1 km zone below the seafloor. Up to this point we have yet to determine what configurations work for identifying both edges. That problem will be addressed in the in the next section. A quality of response column was also included in Table 1. The quality of response was determined qualitatively based on how well defined peaks were relative to what was detected in the surrounding receivers. A moderate response would be when peaks would be seen but on some occasions we see fluctuating responses at other locations. While an excellent quality of response would be when a clear peak is defined without other anomalous surrounding responses detected.

HED Orientation	**RX Measurement**	**Ideal Frequency**	**TX Location**	**Quality of Response**
X	EXEX	$f \geq 0.2$ Hz	Inside disc and near edge	Moderate to poor
X	EYEY	$f \geq 0.2$ Hz	Inside disc and near edge	Moderate to poor
Y	EXEX	All	Inside disc	Excellent
Y	EYEY	0.1 – 0.2 Hz possibly up to 0.5 Hz	Keep at least 1500 m from center of disc (Null coupled positions)	Excellent to Moderate
X/Y	EXEY	None	None	Not usable

Table 1. Ideal Transmitter-Receiver Configurations. Compiled results of ideal transmitter configuration for imaging one edge of a target. The table was constructed based on results from the normalized investigation.

Incomplete Structure Investigation

The results from the normalization investigation suggest that detecting and mapping of sediments is possible with MCSEM. Results from Table 1 also indicate the need for careful selection of proper receiver measurement component, transmitter orientation, location, and frequency in order to image edges. Up to this stage the investigations have been focused primarily on direct imaging of one edge of a shallow hydrocarbon target. The goal of this investigation is to gain some further insight into putting what has been determined in Table 1 and the normalization of responses into practice. In this investigation we attempt to directly image an entire incomplete hydrocarbon disc. This study will also put some perspective on the little known survey design aspects needed for a complete MCSEM survey.

As in the previous studies, a model was constructed to represent an irregular structure. The incomplete structure is centered about the origin of the FE mesh, with primarily three-quarters of a disc structure present. The empty quarter is in the upper left quadrant (quadrant II in the x-y Cartesian plane) and has been refilled with seafloor sediments (σ = 1.0 S/m). The disc had a conductivity of 0.01 S/m, a radius of 2000 m, thickness of 32 m and depth of approximately 525 m.

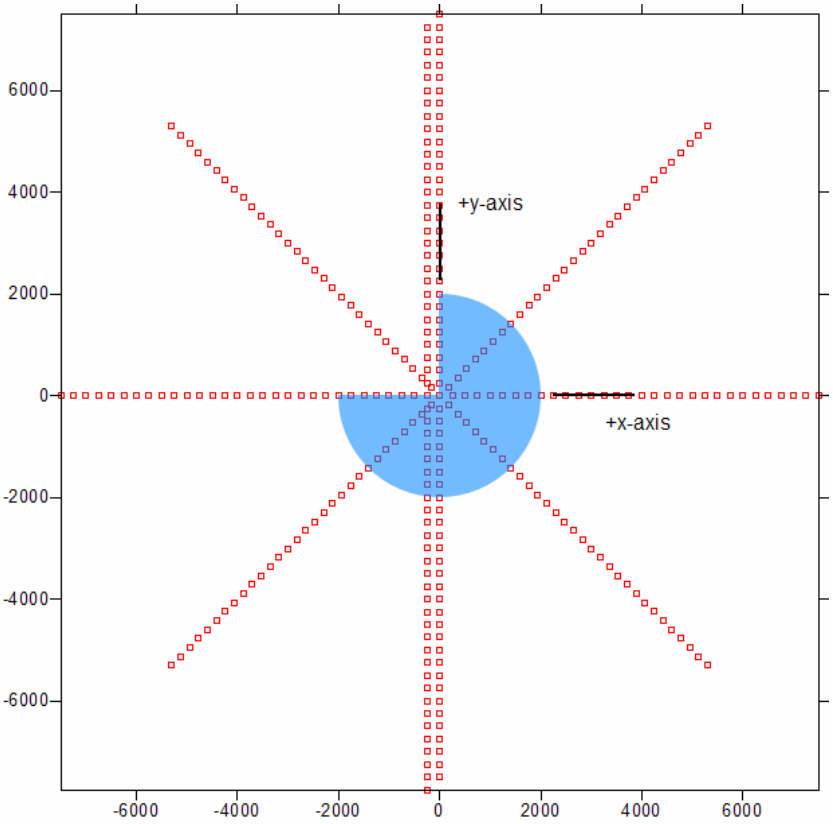

Figure 6. Incomplete Structure Survey Lines**.** Plan view of survey lines of the incomplete disc structure with disc indicated in blue plotted in correct position.

There were eight simulated surveys for each of the four transmitter-receiver configurations, with the exception of Y-HED EYEY which had an extra off-centered survey line (Fig. 6). The four simulated transmitter-receiver pairs are X-HED EXEX, X-HED EYEY, Y-HED EXEX, Y-HED EYEY. The simulated survey had 4 survey lines extending from -10 km to +10 km and was rotated about the origin of the disc. The EXEX survey lines began along the x-axis and were rotated fourth-five degrees clockwise three different times, while the EYEY survey lines begin on the y-axis and were rotated in the same direction. The x-axis stayed as the EXEX line whenever the receiver array was rotated. Unlike the normalization investigation, the receiver array has now been extended from 10 km in length to 20 km, but the receiver separation is still kept at 250 m. From the previous study, careful consideration the X-HED transmitter

orientation leads to the selection of the source frequency of 0.5 Hz while the Y-HED had a frequency of 0.1 Hz. Each survey line had two transmitter positions. For both transmitter orientations, it was positioned at either -1500 m or +1500 m on the x-axis. For the Y-HED EYEY which had a ninth line located 100 m off the y-axis. The transmitter for this line was positioned at x = -1600 m and y = -100 m. For all the survey lines the corresponding double half-space responses were also simulated.

Synthetic survey results for the finite disc were normalized using equation 9 with their corresponding double half-space survey result to create a normalized response curve. The normalized results showed in Fig. 7 and Fig. 8 show varying degrees of success with each transmitter-receiver combination.

The X-HED EXEX configuration (Fig. 7a) is primarily plagued by the problem of not being able to detect the edge of the disc which the transmitter is located immediately over. It was suspected that with this configuration, when the source is located immediately over the receiver we are only detecting the primary field. The primary electric field does not get a chance to penetrate into the disc to excite a secondary field. Another issue that this configuration has is with detecting the incomplete edge. The main problem is a constant response in Fig. 7a is visible over the negative x-axis with no indication of any end to the edge of the disc. The lack of a coherent signal and with the problem of not being able to detect any edges makes this configuration highly unsuitable for direct imaging purposes.

The X-HED EYEY configuration illustrated in Fig. 7b was unable to provide any correct information about the subsurface. Every peak was incorrectly aligned along with unexpected valleys. Thus, it is also highly unsuitable for imaging purposes.

The final line illustrated in Fig. 7c is from the Y-HED EXEX configuration. This configuration similar to X-HED EXEX also suffers from not being able to directly image under the transmitter. However, this configuration as seen from the normalization investigation can easily image the outer radial edge. But when we attempted to image the incomplete edge, it lacks the ability to do so. This configuration can be utilized only in a limited basis for possibly imaging a single edge.

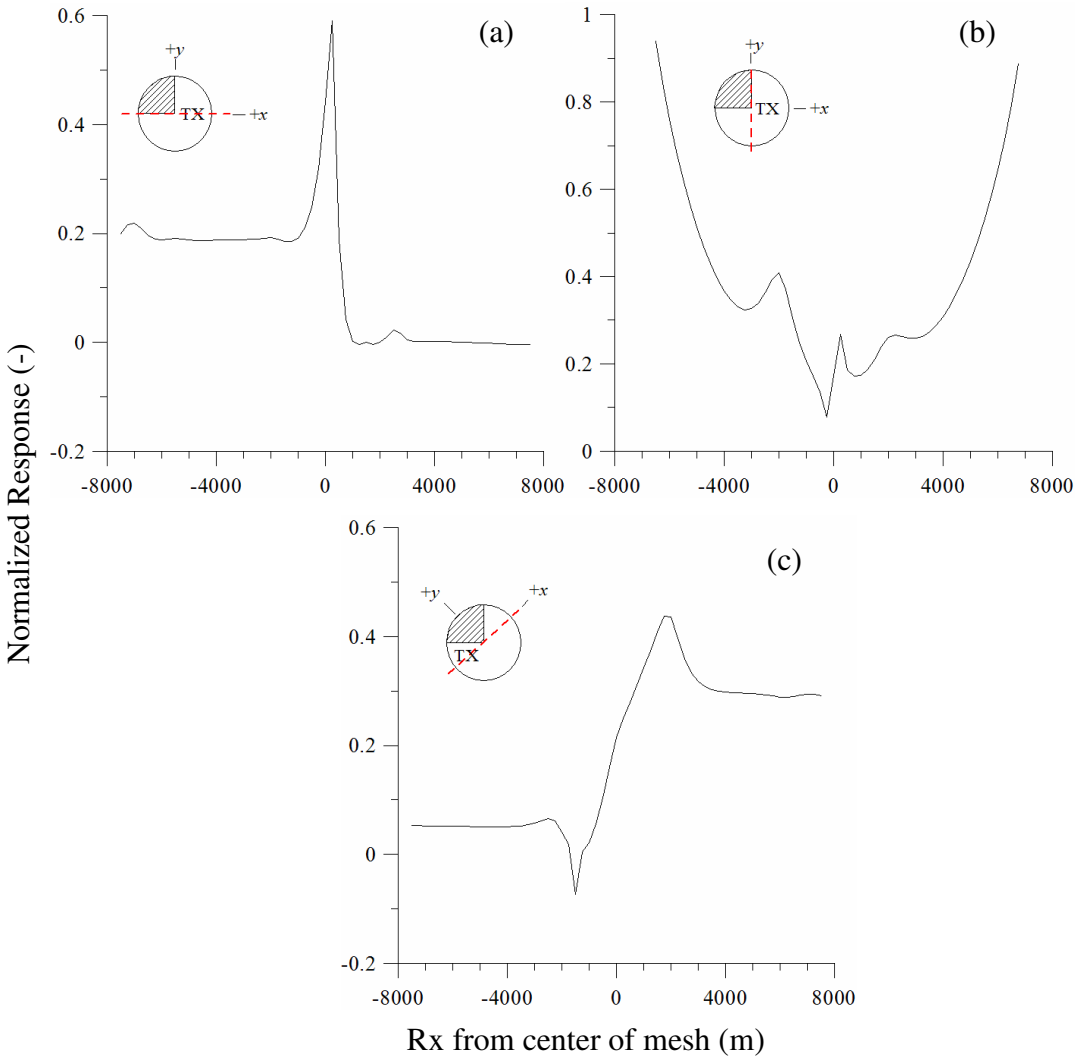

Figure 7. Normalized Results From Incomplete Structure Part 1. Both (a) X-HED EXEX and (b) X-HED EYEY are normalized from a transmitter position of +1500 m and frequency of 0.5 Hz. The lone (c) is from Y-HED EXEX with transmitter frequency of 0.1 Hz and position of -1500 m.

When the receiver array is positioned such as in line four (Fig. 8b) where it crosses the empty quarter, the normalized results produces negative normalized responses in this area. Similar results are confirmed with line nine, the only off-centered

simulated survey line. This is an indication that there is not a need for off-centered lines. However, it was found that transmitter position is extremely important for off-centered survey lines. If the transmitter for line nine was positioned at +1400 m instead of -1600 m, it was found that the receiver array detects a strong influence from the complete portion of the disc. This scenario creates the illusion that two radial edges are present even though there is only a single radial edge and an incomplete inner edge. Also, with an incorrect transmitter position the bottom radial edge was found to be well beyond the +2000 m mark on line nine. This issue may prove to be very problematic with this transmitter and receiver configuration because our studies began with the assumption that our lines were centered over the disc. In a real survey situation this may not be the case. Given that we know that this configuration can at least show both edges, it serves to better image the subsurface than the other configurations.

The final image result when all the normalized survey lines from Y-HED EYEY are compiled and contoured is shown in Fig. 9. The normalized highs correspond exactly to where the lateral radial boundaries are. Associated with the arc of normalized highs, positive non-zero normalized values clearly indicate the inner zone of the disc's presence. While within the empty quarter of the disc the normalization has created a strongly negative peak in that area. The main features of the edges are clearly resolved with the normalized data and the lateral geometry is quantified.

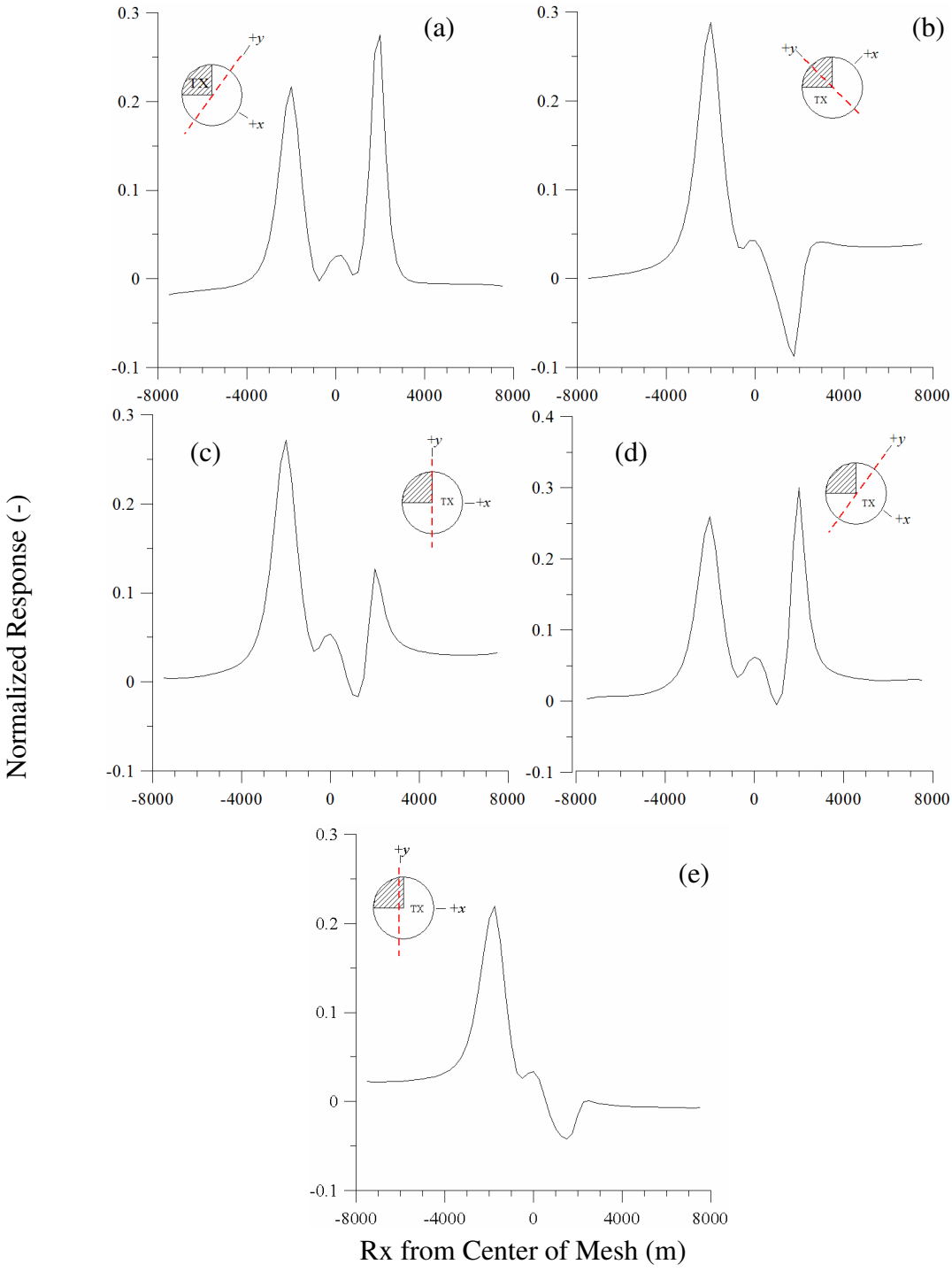

Figure 8. Normalized Results From Incomplete Structure Part 2. These set of graphs are from the Y-HED EYEY configuration with f = 0.1 Hz and Tx = -1500 m or +1500 m (a) Survey line 2; (b) Survey line 4; (c) Survey line 5; (d) Survey line 6; (e) Survey line 9

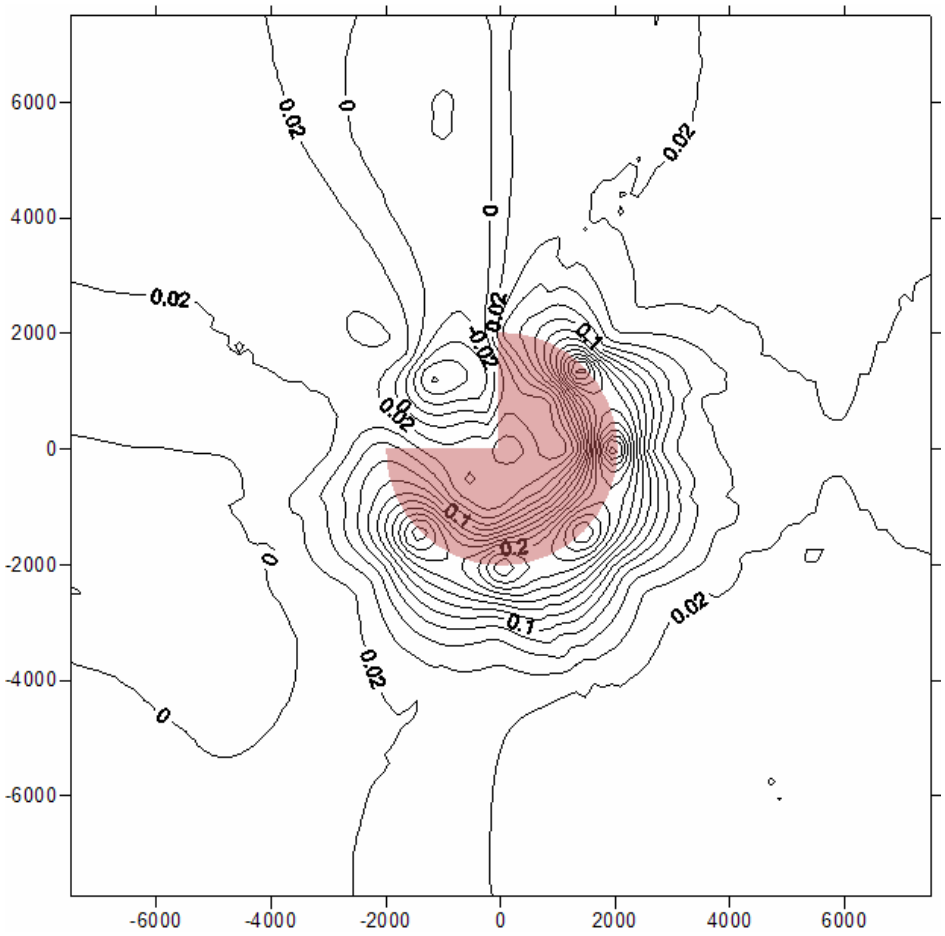

Figure 9. A Plan View Contour of Tabulated Normalized Results for Y-HED EYEY Transmitter-Receiver Configuration. The contour was generated with results from the nine survey lines for this configuration. A transparent pink colored incomplete disc is placed over the contour lines to show the location of its edges.

From the investigations of the incomplete disc, there have been several further discoveries which weren't identified in the normalization investigation. The X-HED EXEX / EYEY and Y-HED EXEX suffer from the problem not being able to completely image both edges of our target. The Y-HED EYEY was the only configuration able to show both lateral extents of the disc. We have seen that there is also not a need for off-centered survey lines. With the last configuration we only need four survey lines rotated about the center of a target with two transmitter positions on either side of a survey line. This would be the most practical and cost-effective scenario in a real MCSEM survey.

CONCLUSION

With fairly simple calculations and careful selection of transmitter location, orientation and frequency, MCSEM sounding can be used to produce an accurate plan view image of the subsurface without the use of inversion modeling. The transmitter-receiver studies here suggest that the Y-HED EYEY configuration is the best in detecting the sharp edges of a hydrocarbon structure. Using this correct configuration, with an operating frequency between 0.1 Hz to 0.5 Hz and positioning the TX at least 1500 m from the center of the disc, this provides the strongest and best response in imaging both edges of the hydrocarbon structure. However in order to image the disc we needed to normalized the response of the disc from that of a known double half-space response with the same transmitter configuration. In reality an off-line survey far removed from the influence of any hydrocarbons needs to be completed for the double half-space response. A possible alternative to the double half-space response used in the normalization is an ocean whole-space response. This could potentially be used to eliminate any chance of bad estimates from the double half-space response in a real survey. It is suggested that future studies should involve the use of an ocean whole-space.

The known lateral extents of our target disc can be used to serve another purpose. 3D heterogeneous inversion typically begins with loosely constrained starting models. However it is probable that the direct imaging result can be used as a fixed constraint for the lateral boundaries thereby reducing the ambiguity associated with complex 3D inversion.

REFERENCES

Badea, E., Everett, M., Gregory, A., and Oszkar, B., 2001, Finite-element analysis of controlled-source electromagnetic induction using Coulomb-gauged potentials: Geophysics, **66**, 786-799.

Bíró, O. and Preis, K., 1989, On the use of the magnetic vector potential in the finite element analysis of three-dimensional eddy currents: IEEE Transaction on Magnetics, **25,** 3145-3159.

Chave, A., and Cox, C.S., 1982, Controlled electromagnetic sources for measuring electrical conductivity beneath the oceans 1. Forward problem and model study: Journal of Geophysical Research, **87**, 5327-5338.

Everett, M.E. and Constable, S., 1999, Electric dipole fields over an anisotropic seafloor: theory and application to the structure of the 40 Ma Pacific Ocean lithosphere: Geophysical Journal International, **136**, 41-56.

Everett, M.E. and Edwards, R.N., 1993, Transient marine electromagnetics – The 2.5-D forward problem: Geophysical Journal International, **113**, 545-561.

King, J., 2004, Using a 3D finite element forward modeling code to analyze resistive structures with controlled source electromagnetics in a marine environment: M.S. thesis. Texas A&M University, College Station, Texas.

Kong, F.N., Westerdahl, H., and Ellingsrud, S., 2002, 'Seabed logging': A possible direct hydrocarbon indicator for deep-sea prospects using EM energy: Oil & Gas Journal 100, **19**, 30-38.

MacGregor, L., and Sinha, M., 2000, Use of marine controlled-source electromagnetic sounding sub-basalt exploration: Geophysical Prospecting, **48**, 1091-1106.

MacGregor, L., Sinha, M., and Constable, S., 2001, Electrical resistivity structure of the Valu Fa Ridge, Lau Basin, from marine controlled-source electromagnetic sounding: Geophysical Journal International, **146**, 217-236.

Unsworth, M., Travis, B., and Chave, A., 1993, Electromagnetic induction by a finite element dipole source over a 2-D earth: Geophysics, **58**, 198-214.

Supplemental Sources

Constable, S., Orange, A., and Hoversten, G., 1998, Marine magnetotellurics for petroleum exploration Part I: A sea-floor equipment system: Geophysics, **63**, 816-825.

Eidesmo, T., Ellingsrud, S., and MacGregor, L.M., 2002, Sea Bed Logging (SBL), a new method for remote and direct identification of hydrocarbon filled layers in deepwater areas: First Break, **20.3**, 144-152.

Farrelly, B., Ringstad, C., Johnstad, S.E., and Ellingsrud, S., 2004, Remote characterization of hydrocarbon filled reservoirs at the Troll Field by Seabed Logging: Paper presented at EAGE Fall Research Workshop, Rhodes, Greece. September 2004.

Flosadóttir, A.H., and Constable, S., 1996, Marine controlled-source electromagnetic sounding 1. Modeling and experimental design: Journal of Geophysical Research, **101**, 5507-5517.

Greer, A.A., MacGregor, L.M., and Weaver, R., 2003, Remote mapping of hydrocarbon extent using marine Active Source EM Sounding: Paper presented at EAGE 65th Conference & Exhibition – Stavanger, Norway. June 2003.

Hoversten, G., Morrison, H., and Constable, S., 1998, Marine magnetotellurics for petroleum exploration, Part II: Numerical analysis of subsalt resolution: Geophysics, **63**, 826-840.

Hoversten, G.M., Constable, S., and Morrison, H., 2000, Marine magnetotellurics for base-of-salt mapping: Gulf of Mexico field test at the Gemini structure: Geophysics, **65**, 1476-1488.

Johnstad, S.E., and Farrelly, B.A., 2005, Seabed Logging on the North Sea Troll Field: Paper presented at 2005 Offshore Technology Conference in Houston, TX. May 2005.

Mitsuhata, Y., 2000, 2-D electromagnetic modeling by finite-element method with a dipole source and topography: Geophysics, **65**, 465-475.

Wicklund, T.A., and Fanavoll, S., 2004, Norwegian Sea: SBL Case Study: Paper presented at 66th EAGE Conference & Exhibition – Paris, France. June 2004.

VITA

Ryan Lau
Email: r2lau@hotmail.com

EDUCATION

Texas A&M University, College Station, TX.
M.S. in geophysics, May 2006

University of Waterloo, Waterloo, Canada.
B.S. in Earth Sciences, May 2004

EXPERIENCE

September 2004 - May 2006	GRADUATE TEACHING ASSISTANT for Dept. of Geology and Geophysics, Texas A&M University, College Station, Texas, USA.
January - August 2003	CO-OP STUDENT: SATELLITE ANALYST, Environment Canada. Toronto, Ontario, Canada.
May - August 2002	CO-OP STUDENT: RESEARCH ASSISTANT for James Sloan, Chemistry Department, University of Waterloo. Waterloo, Ontario, Canada.
January - April 2001	CO-OP STUDENT: GEOPHYSICIST & HYDROGEOLOGIST. Conestoga Rovers & Associates. Waterloo, Ontario, Canada.